Simple Modeling of Particle Trajectories in Solid Rocket Motors

G. Carrier,* F. Fendell,† D. Brent,‡ C. Kimbrough,§ S. Loucks,§ E. Hess,§ and P. Acosta§
TRW Space & Technology Group, Redondo Beach, California 90278

An ultrasimplistic, rapidly executed procedure (with modest computational requirements) is presented for estimating the aluminum-oxide-particle field *within* a long-bore solid rocket motor. The motor has a partially star-configured grain and a re-entrant (submerged) nozzle. The composite grain is of aluminum-particle/ammonium-perchlorate-crystal/rubber-binder type. The first step of the procedure is to obtain an approximate Eulerian solution for the gas-phase flowfield by adapting a simple quasisteady counterflow model; the spatial extent of any recirculatory flow is a parameter of the model, and an axisymmetric equivalent geometry is introduced for the azimuthally periodic corrugations of the star-configured section of the grain. Lagrangian particle tracking within this quasisteady gas-phase flowfield then permits the identification of 1) what fraction of the oxide particles fails to exit the motor and 2) what properties characterize the two-phase flow at the entrance to the sonic nozzle. The sequential calculation outlined here is intended to hold for any degree of velocity slip between the particles and the gas flow, provided the particle loading is not too heavy; in the absence of definite knowledge of the size distribution of the aluminum oxide particles, results are presented in terms of a finite spectrum of discrete particle sizes. Finally, the analysis is generalized to encompass burns during which the rocket motor undergoes rotation about its axis of symmetry.

I. Introduction

CONSIDER a conventional solid rocket motor with a composite-type grain composed of spheroidal ammonium-perchlorate crystals and spheroidal aluminum particles, both enveloped with a rubber binder. In many cases (the ones of interest here), such a motor has 1) a length much greater than the casing diameter, 2) a re-entrant (i.e., submerged) nozzle, and 3) a star-shaped grain nearer to the nozzle (though the grain is azimuthally symmetric further from the nozzle). The star configuration is intended to achieve a solid-to-gas conversion rate that is fairly constant with time during the burn.

The combustion to evolve hot gases occurs in a thin near-grain-surface region, the thickness of which is usually primarily dependent on (and comparable to) the ammonium-perchlorate-crystal size, here O(100 μm).[1] The details of the conversion are not at issue here, and the conversion to products may be taken to occur virtually at the grain-gas boundary. The aluminum (which collectively may constitute about 20% of the total grain mass) combines with oxygen within a few centimeters of the grain-gas boundary to form (usually) molten aluminum-oxide particles (primarily Al_2O_3) of roughly 1-1000-μm size. By stoichiometry, the aluminum-oxide mass constitutes about 38% of the total mass evolved from the grain. Most, but not all, of the aluminum-oxide particles exit the motor with the hot combustion-product gases via the re-entrant nozzle; that small fraction of the particles that do not are observed (in postburn examination) mainly to have impacted the "base" of the motor, where the base is taken to be the portion of the motor casing contiguous to the re-entrant nozzle.

The objective of this study is to furnish a means by which one can estimate the fraction of the aluminum that fails to exit the motor and can identify its origin in the grain. Also, the present study is intended to furnish a means by which one can describe the two-phase flow holding at the "entrance" to the converging-diverging nozzle, so that many already existing hydrocodes may proceed from knowledge of these starting conditions to compute the two-phase flow in the nozzle.[2]

The task is challenging because extremely few experimental data are available either to help resolve the complicated concatenation of processes occurring in the motor or to check the plausibility of predictions from any theoretical model. For example, there are very few reliable data on the spectrum of particle sizes, on the short-time spatial inhomogeneities in the flowfield within the motor ("turbulence"), on the extent of any recirculatory flow,[3] and on the details of the combustion phenomena.

II. Alternative Approaches

In view of the dearth of the observational data, the option adopted here is to develop an ultraconvenient, rapidly solved model of the gaseous flowfield, in terms of as algebraically explicit formulas as are consistent with the simplest reasonable approximations. With such Eulerian expressions for the flowfield, evolved mainly from consideration of the boundary conditions and of the continuity equation (in the small and in the large), the particle trajectories may be obtained by Lagrangian calculation, i.e., by tracking individual particle paths from the grain boundary to their ultimate fate. The final step is to obtain an Eulerian expression for the particle-density field from the Lagrangian calculation. Such an approach is intended to yield results quickly and facilely, with the use of no more than a modest amount of computational effort, so that parametric investigation is feasible.[4] Such parametric investigation might include various casing and nozzle-inlet geometries, variable grain geometries within a given casing-and-nozzle geometry (as the grain burns away with time after ignition), variable total particle loading, and particle-size distribution, etc.

More direct approaches are more computationally demanding, especially since the casing geometry is complicated for a re-entrant nozzle, and the grain boundary is complicated for a star-shaped grain that varies both streamwise and azimuthally.

Received Oct. 30, 1989; presented as Paper 90-0452 at the AIAA 28th Aerospace Sciences Meeting, Reno, NV, Jan. 8-11, 1990; revision received March 5, 1990.

*Consultant, Systems Technology Laboratory.
†Staff Engineer, Systems Technology Laboratory. Associate Fellow AIAA.
‡Subprogram Manager, Systems Technology Laboratory. Member AIAA.
§Member of the Technical Staff, Systems Technology Laboratory.

Retaining compressibility seems nonessential, since (via Bernoulli's equation) the correction to the velocity field owing to variable density is less than 12% if the Mach number does not exceed 0.5—and there is very little, if any, region (*within* the rocket motor, upwind of the nozzle) in which the Mach number exceeds the value 0.5. Thus, in an inviscid approach, one might undertake a finite element solution of the elliptical boundary-value problem describing the vortical flow of interest (taken as quasisteady); however, the vorticity distribution would have to be specified, an arbitrary exercise in the present context.[5] For several vorticity-free flows with specified mass transfer across plausibly configured grain-gas interfaces, the velocity field *has* been obtained by the present authors for long-bore rocket motors with recessed nozzles, by a finite element solution of Laplace's equation. (A numerically obtained potential flow previously has been used for Lagrangian particle tracking in an upper-stage, regressive-burning, shorter rocket motor.[6-8]) This gas-velocity field is virtually duplicated by the approximate solution outlined in the previous paragraph (and developed in Secs. III and IV).

One instead could introduce a pseudoviscosity to describe the generation of vorticity within the rocket-motor flow, but the eddy viscosity is a speculative artifice devoid of fundamental physical foundation, and, in the absence of experimental data, not a viable semiempirical artifice. Effort has been expended to obtain the flowfield in a solid rocket motor in the quasisteady approximation by numerical solution of the laminar viscous equations.[9]

The present approach (of sequentially seeking the velocity field via Eulerian analysis and the particle trajectories by Lagrangian analysis) does encompass any degree of interphase velocity slip, but does not permit (without special provision for iteration) the particle fields to alter the gas-phase flow, as well as vice versa; such more general interaction seems more appropriate for heavier particle loading. However, solving simultaneously for the particle and gas-phase fields (density, velocity, and temperature) results in extensive computation, and the higher-order differencing methods, employed to enhance accuracy, seem to incur numerically introduced oscillatory behavior in the results.[10,11] Only in the asymptotic limits of indefinitely small slip, or of indefinitely large slip, between the gas and particulate phases is an analytic treatment of a coupled, Eulerian formulation usually possible, and behavior in these limits can often be anticipated.

III. Model for the Gas-Phase Flowfield

For a long-bore composite-grain rocket motor with a cylindrically symmetric casing and nozzle, the pressure and temperature within the rocket motor are taken to be spatially uniform and (tentatively) known as a function of time. The gas-phase density is then spatially uniform and known as a function of time from the ideal-gas equation of state, in which a constant "average" molecular weight is adopted.

The rate at which the solid grain is gasified, i.e., the grain-surface regression rate, is taken to be given by an empirically

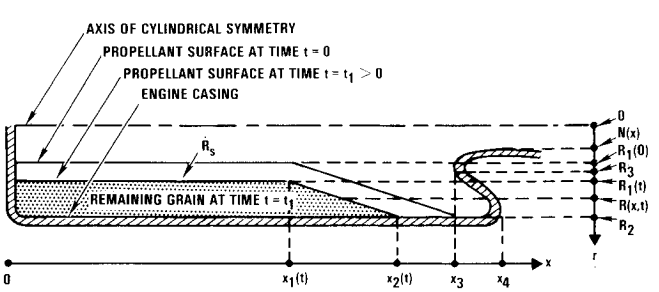

Fig. 1 Geometry (not to scale) of a motor with a re-entrant nozzle. Over the axial span $x_2(t) > x > x_1(t)$, the grain is star-shaped, at least at early times after ignition (at $t = 0$). For $x_1(t) > x > 0$, a cylindrical bore exists: the radius (of the circle-equivalent gas-filled area) $R(x,t) \to R(t)$.

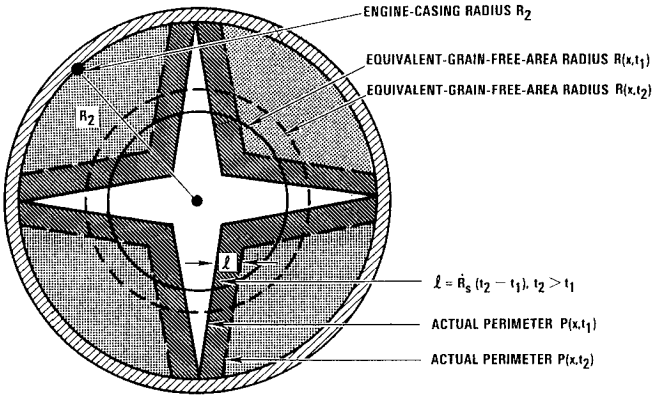

Fig. 2 A cross section (perpendicular to the axis) in the domain $x_2(t) > x > x_1(t)$, showing 1) the star configurations at time $t = t_1$ (solid lines) and at time $t = t_2$ ($> t_1$) (dashed lines), and 2) the radii of the circle-equivalent, gas-filled areas. At this x, a deeply cut star exists.

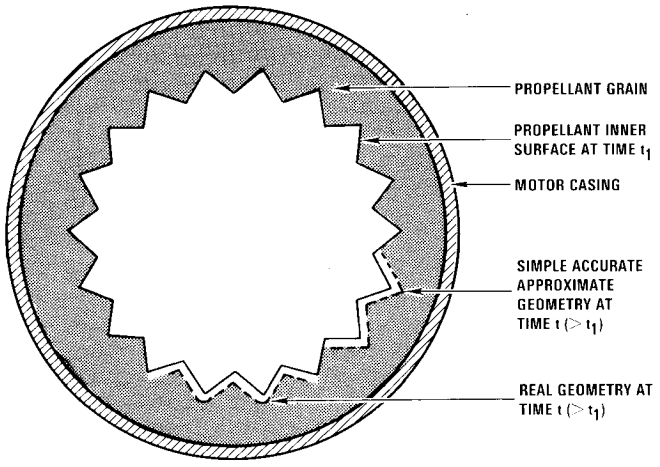

Fig. 3 Actual time evolution of a "shallow-star" geometry, with arcs, and a simplification preserving the "outer points" (outer vertices) of the star.

known function of pressure and thus is implicitly specified as a function of time. The efflux (mass per area per time) from the grain boundary evolves perpendicular to the grain boundary, with the gas conveying a greater portion of the efflux and the particles, a smaller portion of the efflux. The grain is modeled as homogeneous except on the aluminum-particle-size microscale, and the oxygen content of the grain is such that (spherical) aluminum-oxide particles (in general, with a broad range of radii) are formed at the grain-gas interface; these particles at the boundary are taken to have no motion, and are accelerated by the gas motion.

In the laboratory frame of reference (as opposed to a grain-boundary-fixed frame of reference), the grain surface retreats, along the local normal to its instantaneous position, at the gasification rate. Since the position of the gas-grain interface is given at the time of ignition, $t = 0$, a new configuration can be evolved from the previous configuration by integration over time of the gasification rate $\dot{R}_s[p(t)]$ (Fig. 1). In this manner the area of the cylindrically symmetric portion of the grain-gas interface increases monotonically in time (until no grain surface remains because the radius of the grain-gas boundary becomes coincident with the inner radius of the casing). In contrast, the surface area of the sawtooth-like, star-configured portion of the combusting grain boundary decreases monotonically in time (Fig. 2). For the convenience of a cylindrically symmetric analysis, an "equivalent-bore-area" cylindrical radius (with an "enhanced" perimeter) may be adopted as an approximation to the actual star-configured cross section. Alternatively, the enhanced efflux from the star-configured cross

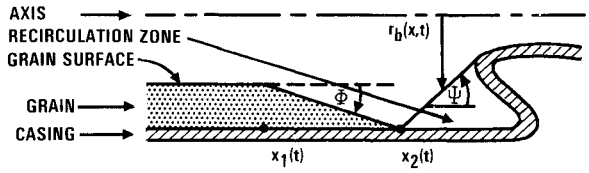

Fig. 4 The star-configuration-associated angle $\Phi(x,t)$, fairly adequately approximated as independent of the axial coordinate x; and the angle $\Psi(x,t)$, associated with the recirculation-zone boundary $r_b(x,t)$. We adopt $\Psi(t)$, a conically shaped boundary; here $F = 1$, i.e., the conical boundary intersects the casing at $x = x_2(t)$. For $0<F<1$, the intersection occurs at $x_2(t)<x<x_3$.

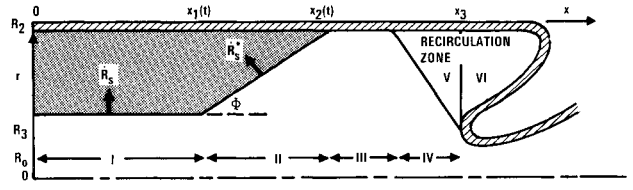

Fig. 5 Idealized motor geometry (not to scale) for the flow model of the Appendix. The recirculation zone (regions V, VI) has zero gas velocity; here, $F \doteq 0.5$, i.e., the recirculation-zone boundary intersects the casing midway between $x_2(t)$ and x_3. The star configuration $[x_1(t)<x<x_2(t)]$ is subsumed by a conical surface with enhanced-regression rate $\dot{R}_S^*$.

section may be simulated within an axisymmetric model by adoption of an enhanced gasification rate $\dot{R}_S^*[p(t)]$, the adopted conical surface having a perimeter with an axially varying radius that is a simple linear interpolation between 1) the radius at the axial position $x_1(t)$, the downstream end of the constant-radius, cylindrical-bore portion of the combusting grain boundary and 2) the radius at the axial position $x_2(t)$ at which the radius of the star-configured cross section becomes coincident with the inner radius of the casing. Both these axisymmetric approximations for the star-configured region are considered below.

It is convenient to identify $x = 0$ as the axial position of the head wall of the rocket motor; $x = x_3$ as the plane (perpendicular to the axis of symmetry) marking the entrance to the re-entrant nozzle; $x = x_4$ as the plane (perpendicular to the axis of symmetry) marking the downwindmost position of any point on the inner lining of the rocket-motor base. In general, $x_4>x_3>x_2(t)>x_1(t)>0$. For a "simple" rocket motor without a re-entrant nozzle, $x_3 = x_4$.

It is helpful to define the following (cylindrical) radial distances: $r = R_1(t)$ is the radius of the combusting grain surface for $0<x<x_1(t)$; $r = R_2$ is the inner radius of the casing; and $r = R_3$ is the radius of the nozzle at $x = x_3$. The position $r = R(x,t)$ is the position of the effective cylindrical radius (at axial position x, at time t) defining the area accessible to the solid-grain-evolved gases in the motor. For example, for $x>x_3$, $R(x,t) = N(x)$, the radius of the nozzle.

A simple, inviscid, cylindrically symmetric counterflow provides a basic approximation to the gas-phase velocity field in the present concept. In $x_1(t)>x>0$, a radial influx off the grain boundary becomes an axial flow toward the nozzle, in accord with continuity; this model is adapted for $x_2(t)>x>x_1(t)$. Whether or not there is a re-entrant nozzle, a recirculation zone [occupying *some* of the gas-filled volume included within the domain $x_2(t)<x<x_4$, $R_3<r<R_2$] is expected, although its extent is uncertain.[3]

For a simple motor with a constant-radius bore, Culick[12] postulates a distributed vorticity field for which zero slip holds at the grain-gas interface in an inviscid counterflow. Conventionally for inviscid flow, a vortex sheet is introduced at the boundary to enforce zero slip.[13] In any case, Culick's model is no less ad hoc, but is less tractable, than the present vorticity-free inviscid counterflow.

The gas-phase velocity field need be delineated only to the accuracy deemed adequate for predicting particle trajectories. It is taken that any particle that enters the recirculation zone never exits via the nozzle, but rather impacts on the base of the casing (or inelastically on the sidewall of the casing very near the base). Since the precise point of impact is not crucial, the gas-phase velocity field within the recirculation zone is approximated to be null; i.e., if the gas-phase velocity is

$$v(r,x,t) = v(r,x,t)\hat{r} + u(r,x,t)\hat{x} \tag{1}$$

where u is the axial velocity component and v is the radial velocity component in the swirl-free flow, then $u = v = 0$ in the recirculation zone. The sensitivity (of the fraction of the particles that fail to leave the motor) to the assignment of boundaries to the recirculation zone is to be investigated parametrically. Rigorously, no combustion gas enters the recirculation zone in the present model, which is quasisteady with respect to the gas-phase velocity field; whatever gas is in the recirculation zone was "always there." The recirculation-zone/combustion-gas interface is a streamsurface.

IV. Solution for the Gas-Phase Velocity Field

From knowledge of the initial position of the inner surface of the grain, one may calculate the area $A(x,t)$ of the grain-free cross section and the total grain-gas perimeter $P(x,t)$. An equivalent axisymmetric configuration is adopted for the star-configured, azimuthally periodic portion of the geometry, by defining an equivalent (cylindrical-polar-coordinate) radius for the grain-gas boundary. Thus, by definition,

$$R(x,t) = \left[A(x,t)/\pi\right]^{1/2}, \qquad x_2(t)>x>0 \tag{2a}$$

$$P(x,t) \geq 2\pi R(x,t), \qquad R\left[x_2(t),t\right] = R_2 \tag{2b}$$

defines $x_2(t)$ uniquely for the grain geometries of interest here. [In the bore region $x_1(t)>x>0$, $A(x,t)\to A(t)$ so $R(x,t)\to R(t)$.] The temporal evolution of the gas-grain boundary for the star-configured domain $x_2(t)>x>x_1(t)$ is such that a finite curvature evolves at those positions of the combusting grain surface closest to the casing (unless the star "cuts" are so "deep" into the grain that the "points" of the star are initially on the inner lining of the casing, at the axial

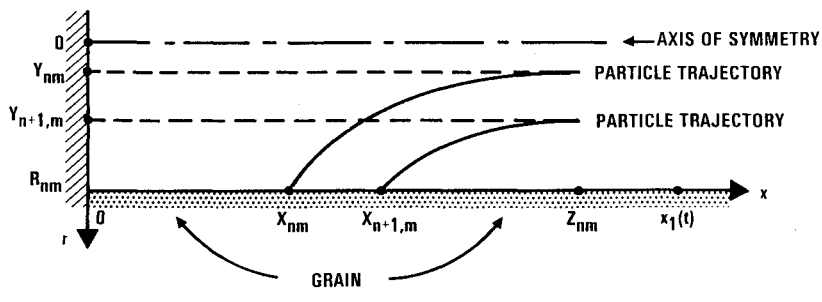

Fig. 6 Two hypothetical (but plausible) particle trajectories, from which the Eulerian particle-density field ρ_p may be approximated for the intermediate radial positions at the axial position $x = Z_{nm}$.

position under discussion). Meticulously, the subsequent grain configuration (Fig. 3) evolves to a sequence of straight-line segments joining arcs with centers at the original points of the star, the radius of each arc being given by the integral over time (since $t=0$) of the quantity $\dot{R}_s[p(t)]$. However, it suffices to extend the straight-line segments near the evolved points as in Fig. 2. In any case, the peripheral calculations to obtain $R(x,t)$ and $P(x,t)$ have now been defined.

If the area of the propellant surface in the range from x to $(x+\mathrm{d}x)$ is denoted $B(x,t)$, then (Figs. 4, 5) with $R_x(x,t)<\infty$,

$$B(x,t)=P(x,t)\,\mathrm{d}x/\cos\Phi(x,t),\quad \tan\Phi(x,t)=\frac{\partial R(x,t)}{\partial x} \tag{3}$$

The volume loss (per time) of propellant, owing to the recession of the grain boundary at speed $\dot{R}_s(p)$ in a direction perpendicular to the old and new boundary, is $\dot{R}_s(p)B(x,t)$. The mass of gas supplied by the propellant in the interval $\mathrm{d}x$ per unit time is denoted $\dot{m}(x,t)$:

$$\dot{m}(x,t)=\rho_1\dot{R}_s(p)P(x,t)/\cos\Phi(x,t)=\rho_1\frac{\partial A(x,t)}{\partial t} \tag{4}$$

where ρ_1 is the mass of propellant that turns into gas per unit volume of propellant. The integral of $\dot{m}(x,t)$ over all x for which a combusting grain-surface perimeter $P(x,t)$ exists at time t gives the mass of gas per time entering the nozzle.

Whereas the time t is an independent variable (along with the axial distance x) for the propellant-grain geometry properties $A(x,t)$, $P(x,t)$, and for the mass input to the core region $\dot{m}(x,t)$, the time t is ascribed only a parametric role for obtaining the gas-phase (Eulerian) velocity components $u(r,x,t)$ and $v(r,x,t)$. Because of the confining geometry, to satisfactory approximation for present purposes,

$$u(r,x,t)=u(x,t),\qquad v(r,x,t)=rw(x,t) \tag{5}$$

Conservation of mass in the small is expressed by

$$(\rho ru)_x+(\rho rv)_r=0 \tag{6a}$$

or

$$(\rho u)_x+2\rho w=0 \tag{6b}$$

For conservation of mass in the large under Eq. (5), one considers a volume of the rocket-motor core bounded axially by planes at x and $(x+\mathrm{d}x)$ and laterally by the (equivalent) perimeter $r=R(x,t)$. At time t, the mass flux out of the volume at $(x+h)$ minus the mass flux into the volume at x plus the rate of increase of mass inside the volume equals the rate of mass supply by the propellant grain:

$$\rho(t)u(x+h,t)A(x+h,t)-\rho(t)u(x,t)A(x,t)+\frac{\partial}{\partial t}\int_x^{x+h}\rho(t)A(x_1,t)\,\mathrm{d}x_1=\int_h^{x+h}\left\{\rho_1\dot{R}_s[p(t)]P(x_1,t)/\cos\Phi(x_1,t)\right\}\mathrm{d}x_1 \tag{7a}$$

On dividing by h and taking the limit as $h\to 0$, one obtains

$$(\rho uA)_x+(\rho A)_t=\rho_1\dot{R}_sP/\cos\Phi \tag{7b}$$

$$\rho(t)u(x,t)=\frac{1}{A(x,t)}\int_0^x\left[(\rho_1\dot{R}_sP/\cos\Phi)-(\rho A)_t\right]\mathrm{d}x_1 \tag{7c}$$

since $u(0,t)=0$. The quantity $A(x,t)$ and the integrand are known for each x and t, and so the integration gives the product $\rho(t)u(x,t)$ for each x and t; the product $\rho(t)w(x,t)$ then follows from Eq. (6b).

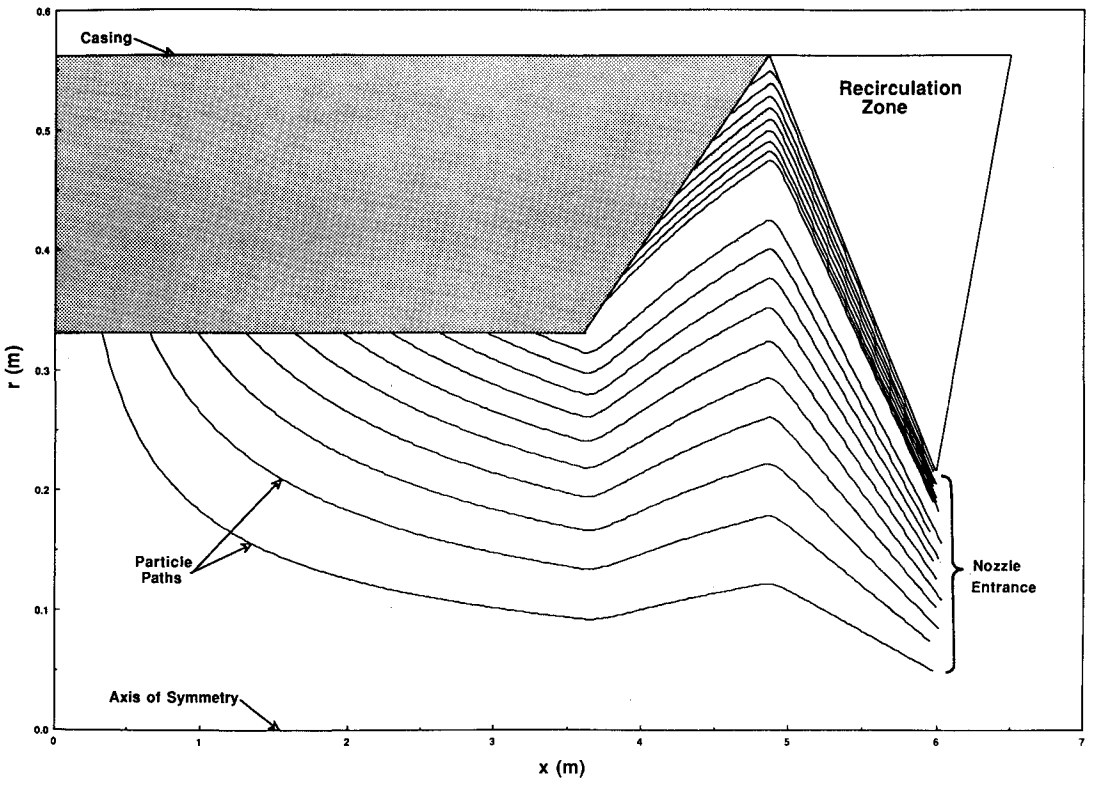

Fig. 7 Trajectories of particles emerging from the gas/grain interface at time t = 20 s for the case of Eq. (30), for particles with a diameter of 50 μm. Virtually all of these particles exit via the nozzle.

The boundary $r_b(x,t)$ of the recirculation zone here is taken to be a conical surface extending from some circle on the casing $\{R_2, x_3-[x_3-x_2(t)]F\}$, $0<F<1$, to the circle chosen to demarcate the nozzle entrance (R_3,x_3); investigation of the sensitivity of the results to the extent of the recirculation zone is here limited to the adoption of various (fixed) values of the factor F. [Clearly, other configurations for the boundary, a different definition of the nozzle entrance, and a temporally variant factor F could have been considered. For example, one could have required that the circle on the casing demarcating the recirculation zone track the retreating grain extremity $x_2(t)$ for some prespecified time interval into the burn, and then after remain fixed.] Thus, in

$$\left\{x_3-\left[x_3-x_2(t)\right]F\right\} \le x \le x_3, \qquad A(x,t)=\pi\left[r_b(x,t)\right]^2 \quad (8)$$

and Eqs. (7c) and (6b) continue to hold. More explicitly,

$$v(r,x,t)=v\left[r_b(x,t),x,t\right]\frac{r}{r_b(x,t)}, \qquad 0\le r\le r_b(x,t) \quad (9a)$$

where

$$-v\left[r_b(x,t),x,t\right]=u\left[r_b(x,t),x,t\right]\tan\Psi(x,t) \quad (9b)$$

and $\left[\left|dr_b(x,t)/dx\right|<\infty\right]$

$$\tan\Psi(x,t)=-\partial r_b(x,t)/\partial x \quad (9c)$$

$$u\left[r_b(x,t),x,t\right]=u(x,t), \qquad 0\le r\le r_b(x,t) \quad (10)$$

For conditions of practical interest, the time-derivative term in Eq. (7c) often is negligible.

The alternative treatment (of the gas-phase flowfield) mentioned in the third paragraph of Sec. III is developed in the Appendix.

V. Self-Consistency of a Rocket-Motor/Nozzle-Flow Analysis

The variation in the (spatially uniform) pressure field in time is not large after the initial transient, but the above quasisteady approach, wherein the solution in space is sought for the gas flow at each of a finite number of sequential times as the grain geometry evolves, can be refined as follows. At ignition, $t=0$, let $p=p_1$ (given); from $\dot{R}_s(p_1)$, the quantities ρu and ρw are obtained for the first time interval at all axial positions from Eqs. (7c) and (6b). For the second time interval, one seeks an updated value of ρ consistent with the temperature (given as a function of time only) and with the values just found for ρu and ρw; this updated value of ρ gives an updated value of $\dot{R}_s$, and, again from Eqs. (7c) and (6b), values at all x for ρu and ρw for that second time interval. The details of this updating of the pressure field are more readily delineated once the flow in the nozzle becomes sonic (an event that typically occurs very soon after ignition, relative to the duration of the burn), because thenceforth the stagnation pressure p_{st} at $x=0$ has to be taken to be consistent with a sonic condition. Probably there is no need for iterative calculation at a given time into the burn, but the need for self-consistency (for analyses in which the in-motor calculation and in-nozzle calculation are executed sequentially) seems worth noting.

For a sonic nozzle, for an ideal gas,

$$c_pT_{st}=Q \quad (11)$$

$$a_{st}^2=\gamma RT_{st} \quad (12)$$

where c_p is the (constant) specific heat at constant pressure for the gas, T_{st} the stagnation temperature, Q the heat of combustion per mass of gas (large relative to the ambient enthalpy), γ the ratio of specific heats, R the particular gas constant, and

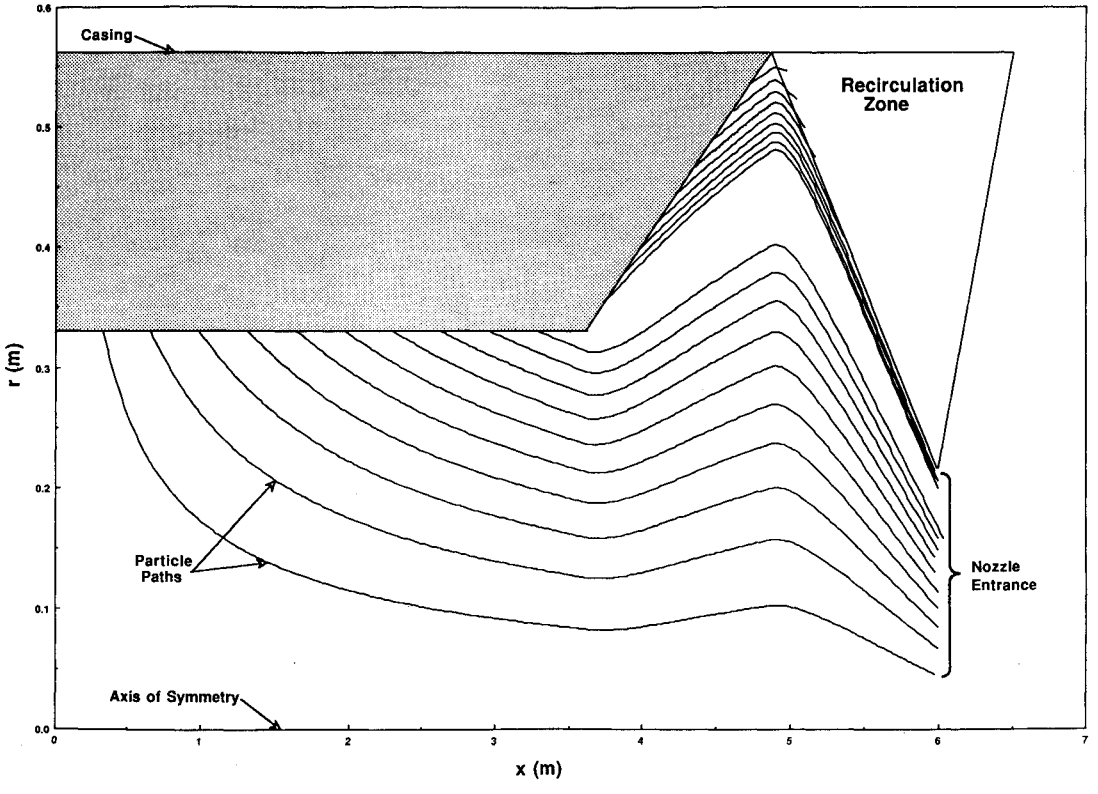

Fig. 8 Trajectories of particles emerging from the gas/grain interface at time t = 20 s for the case of Eq. (30), for particles with a diameter of 100 μm. Many of the particles emerging from the conical section of the grain enter the recirculatory-flow region.

a_{st} the speed of sound at the temperature T_{st}. By Bernoulli's relation, if $q^2 = u^2 + v^2$, and a is the speed of sound,

$$\frac{a^2}{a_{st}^2} = 1 - \frac{\gamma - 1}{2}\left(\frac{q^2}{a_{st}^2}\right) \tag{13}$$

At the throat of the nozzle $q^2 = a^2 = a^{*2}$, so Eq. (13) gives

$$a^{*2} = \frac{2}{\gamma + 1} a_{st}^2 \tag{14}$$

Since $T \sim \rho^{(\gamma-1)}$ for adiabatic flow of an ideal gas, that last relation, by use of Eqs. (11-13), may be written as

$$\rho^* a^* = \left[2/(\gamma+1)\right]^{(\gamma+1)/[2(\gamma-1)]} \rho_{st} a_{st} \tag{15}$$

But $\rho^* a^* A^*$ is the (tentatively calculated) total mass flux at the throat; since a^* and A^* are known, then ρ^* is known, and, from Eq. (15), so is ρ_{st}. From the equation of state, one obtains p_{st}:

$$p_{st} = \rho_{st} a_{st}^2 / \gamma \tag{16}$$

The consistency check is whether the value of p_{st} from Eq. (16) is consistent with the value used to obtain the total mass flux at the throat.

VI. Lagrangian Tracking of Particle Trajectories

If X is the axial coordinate of a particle and Y is the radial coordinate, then the equations describing the motion of a spherical (nonlifting) particle in the previously discussed gaseous flow, in the absence of significant effects from gravitational acceleration or from particle-particle collisions, are

$$\mu X_{tt} = D(u - X_t) \tag{17a}$$

$$\mu Y_{tt} = D(v - Y_t) \tag{17b}$$

Here subscript t refers to a total derivative, μ is the mass of a particle (a sequence of monodisperse distributions is undertaken to investigate a polydisperse distribution), and D is the drag coefficient. If the spherical particle is in Stokes flow, $D = 6\pi\mu_g a$, where μ_g is the dynamic viscosity of the gas, and in this section the quantity a is the particle radius. The particle-relaxation time $\tau_p \doteq (2/9)(a^2/\nu)(\rho_s/\rho)$ where ν is the kinematic viscosity of gas and ρ_s is the (true) density of the solid-particle matter. A typical flow time $\tau_f \doteq (R/\dot{R}_s)(\rho/\rho_s)$. The so-called Stokes number $\tau_p/\tau_f \doteq (2/9)(a^2/\nu)(\dot{R}_s/R)(\rho_s/\rho)^2$. For small values of the Stokes number, typical of sufficiently small particles, the particle is rapidly brought to the local-gas-flow speed (on the time scale τ_p), and thenceforth slip of the particle relative to the local gas flow is negligible. The small-particle limit is typical of singular-perturbation conditions: a so-called "stiff" differential equation requires special numerical treatment, but here the behavior of the solution is readily apparent analytically. For large values of the Stokes number, typical of sufficiently large particles, the particle proceeds in accord with its injection velocity, and there is very large slip of the particle relative to the local gas flow; for an initially motionless particle, movement is imparted only on the long time scale $\tau_f^{3/2}/\tau_p^{1/2}$.

Equations (17a) and (17b) hold if the Reynolds number $Re < 2$, where, by definition,

$$Re = \frac{2a\rho_g}{\mu_g}\left[(u - X_t)^2 + (v - Y_t)^2\right]^{1/2} \tag{17c}$$

More generally, the Stokes-drag-containing relations of Eqs. (17a) and (17b) are taken to be[14]

$$\mu X_{tt} = \left[C_D(Re)\right]\left(\frac{\pi\mu_g a}{4}\right) Re(u - X_t) \tag{17d}$$

$$\mu Y_{tt} = \left[C_D(Re)\right]\left(\frac{\pi\mu_g a}{4}\right) Re(v - Y_t) \tag{17e}$$

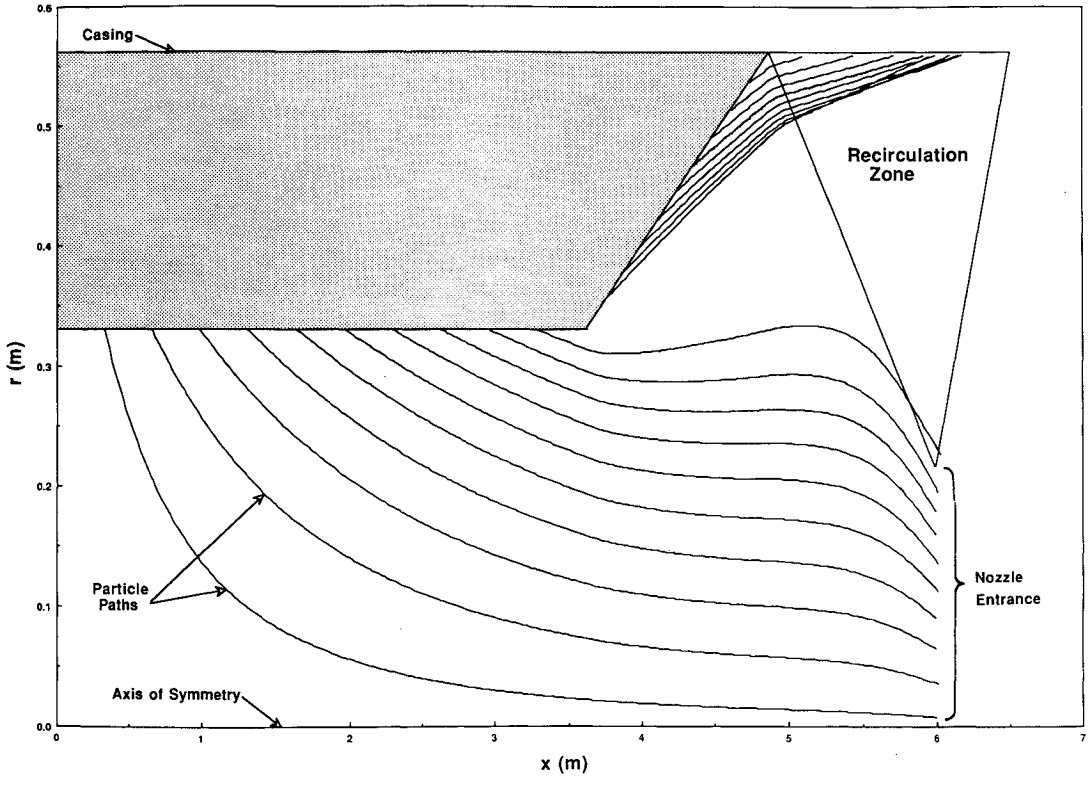

Fig. 9 Trajectories of particles emerging from the gas/grain interface at time t = 20 s for the case of Eq. (30), for particles with a diameter of 500 μm. Many of the particles from the conical section penetrate to the side-wall lining, and some from the downwind end of the bore section penetrate to the base lining.

where the drag coefficient $C_D(Re)$ is taken to be[15]

$$C_D(Re) = \begin{cases} 24/Re, & Re < 2 \\ 18.5/Re^{0.6}, & 2 < Re < 500 \\ 0.44, & 500 < Re < 2 \times 10^5 \end{cases} \quad (17f)$$

Let X_{nm} be the location of particle (n,m) at axial coordinate $x = X_n(t_m)$ and at radial coordinate $r = R(X_n, t_m)$. That is, the particle is on the gas-grain interface at $x = X_n$ at $t = t_m$ (whence X_{nm}) and hence has radial position $R(X_n, t_m) = R_{nm}$. For times after the time at which the particle leaves the gas-grain interface, its axial position is denoted by (a different symbol than X, specifically) Z; the subsequent radial coordinate Y has already been introduced. Thus, $Z_{nm}(t)$ is the axial coordinate, and $Y_{nm}(t)$ is the radial coordinate at time t of a particle that starts from (R_{nm}, X_{nm}). Hence, Eqs. (17a) and (17b) become

$$\mu \ddot{Z}_{nm} = D\left[u(Y_{nm}, Z_{nm}) - \dot{Z}_{nm}\right] \quad (18)$$

$$\mu \ddot{Y}_{nm} = D\left[v(Y_{nm}, Z_{nm}) - \dot{Y}_{nm}\right] \quad (19)$$

The associated initial constraints state that the solid particle is motionless as the solid boundary recedes past it:

$$Z_{nm}(t_m) = X_n(t_m) = X_{nm}, \qquad \dot{Z}_{nm}(t_m) = 0 \quad (20)$$

$$Y_{nm}(t_m) = R_{nm}, \qquad \dot{Y}_{nm} = 0 \quad (21)$$

Consider numerical integration to have yielded $Z_{nm}(t), Y_{nm}(t)$ for the discussion that follows.

Among all the particles that "begin" at time t_m, those at the point $X^*(t_m), R^*(t_m)$ have a trajectory that just grazes the surface at the inlet to the re-entrant nozzle. Such particles can be picked out of the results for the family of calculations for all n at the particular time t_m. For the quasisteady hypothesis adopted here, the flux of particles through the nozzle "at time t_m" is the flux of particles out of the propellant over the grain-gas interface for $X^*(t_m) > x > 0$; the flux of particles out of the propellant over the grain-gas interface for $x_2(t_m) > x > X^*(t_m)$ does not enter the nozzle, but instead impacts on some surface within the motor. *If* typically one-third of the mass of the solid propellant becomes particulate, then the flux of particles from the grain-gas boundary from $X^*(t_m) > x > 0$ is just one-half of the flux of gas from that same part of the boundary "at that time." In turn, that partial gas flux is equal to the quantity

$$2\pi \int_0^{X^*(t_m)} R(x, t_m) \dot{m}(x, t_m)\, dx$$

where $\dot{m}(x,t)$ is given by Eq. (4). A subsequent integration over time from $t = 0$ to burnout time gives twice the total mass of particulate entering the nozzle.

For purposes of calculating what fraction of the mass of the grain enters the nozzle, one need identify the position $X^*(t_m)$ only, and results obtained for a preceding time should limit the number of trajectories that need be calculated for a subsequent time. The more general task of obtaining a detailed description of the particle-phase-density field throughout the motor requires calculation of many further trajectories.

It is anticipated that particles evolved from the constant-bore-radius portion of the grain may tend to collect in a small-radius core near the axis of symmetry; this core probably increases in radius with distance downwind. *If* a particle effectively reaches the axis of symmetry, that particle may be taken to move thenceforth downwind on the axis; possible singular artifacts of the model are thereby obviated with no compromise in practical results.[16] In fact, it seems worth identifying the axial position $X^+(t_m)$, associated with $R^+(t_m)$, where the particle emerging from the cited circle on the grain boundary has a trajectory that just skims the axis of symmetry as the particle reaches the entrance to the re-entrant nozzle. The radial profile of the particle-density field at the nozzle entrance may be obtained by examining the trajectories characterized by a starting position on the grain boundary within the range $X^*(t_m) > X_{nm} > X^+(t_m)$.

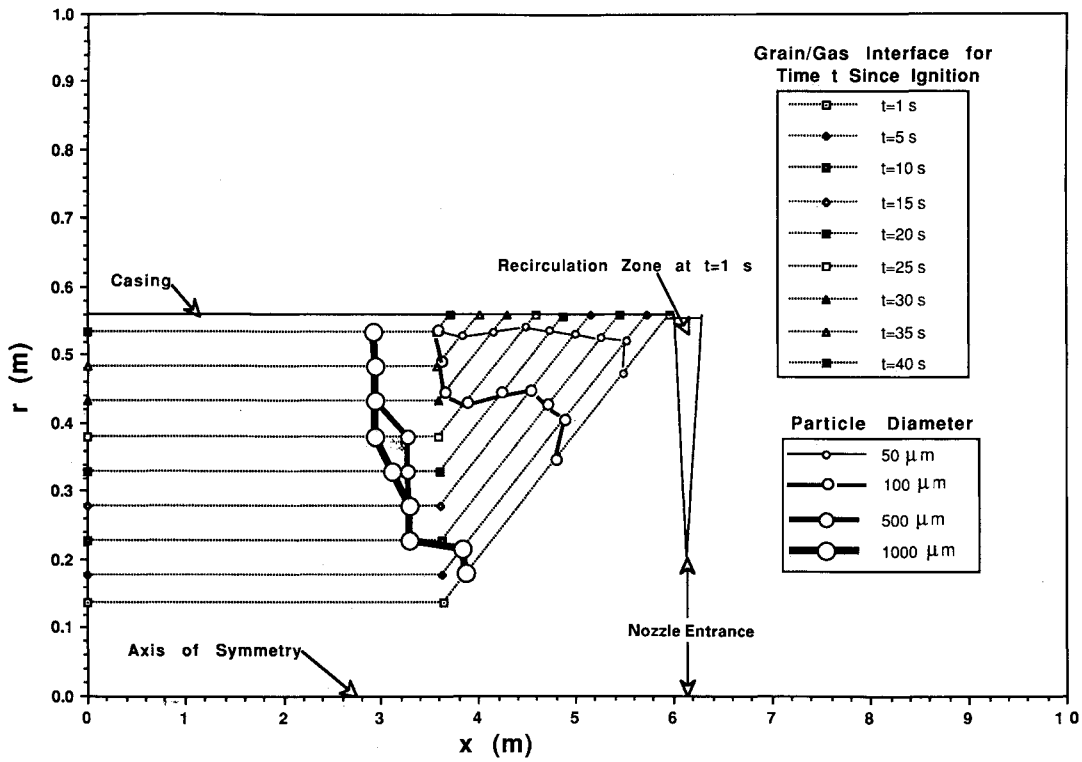

Fig. 10 The temporal evolution of the gas/grain interface, and of the "separatrices" that distinguish the motor-exiting particles emerging more upwind along the interface from nonexiting particles emerging more downwind, for four particle sizes, for the case of Eq. (30).

As an exemplary calculation for ascertaining the Eulerian particle density $\rho_p(r,x,t)$ from the Lagrangian particle-trajectory results, attention is confined to the bore region of the gas-phase flow $x_1(t)>x>0$. Suppose (Fig. 6) that the particle (R_{nm},X_{nm})—discussed in Eqs. (18-21)—achieves at time $T(>t_m)$ position (Y_{nm},Z_{nm}), and the particle $(R_{nm},X_{n+1,m})$ later achieves position (Y_{n+1},Z_{nm}), where $X_{n+1,m}>X_{nm}>0$, $Y_{n+1,m}>Y_{nm}>0$, and $x_1(t_m)\geq Z_{nm}>X_{n+1,m}$. Since the mass flux of particles through the plane Z_{nm} between the radii Y_{nm} and $Y_{n+1,m}$ equals the mass flux through the combusting-grain-surface boundary R_{nm} between the axial positions X_{nm} and $X_{n+1,m}$, a tedious but straightforward way to identify the Eulerian particle density near position (Y_{nm},Z_{nm}) evolves—and the accuracy is increased as $X_{n+1,m}\to X_{nm}$ so that (presumably) $Y_{n+1,m}\to Y_{nm}$. Explicitly, one may obtain $\rho_p(Y_{nm},Z_{nm},T)$ from the relation

$$(X_{n+1,m}-X_{nm})\left[(\rho_{sg}-\rho_1)/\rho_1\right]\dot{m}(X_{nm},t_m)$$
$$\doteq 2\pi Y_{nm}(Y_{n+1,m}-Y_{nm})\dot{Z}_{nm}(T)\rho_p(Y_{nm},Z_{nm},T) \qquad (22)$$

where $\dot{m}[X_{nm},t_m]$ is defined in Eq. (4), ρ_1 is recalled to be the density of the solid grain that "emerges" as gas, and ρ_{sg} is the (total) density of the solid grain.

VII. Generalization for a Rotating Motor Case

The previous development for the radial and axial velocity components may be taken to continue to hold for a highly subsonic flow in which the pressure field is satisfactorily approximated as spatially homogeneous. However, the gas-phase velocity field of Eq. (1) is now generalized to include a swirling speed w in the azimuthal direction $\hat{\theta}$:

$$v(r,x,t)=v(r,x,t)\hat{r}+w(r,x,t)\hat{\theta}+u(x,t)\hat{x} \qquad (23)$$

where, if Ω is the angular velocity of the casing and grain,

$$w(r,x,t)=\Omega(t)\left[R(x,t)\right]^2/r \qquad (24)$$

In practice, diffusive effects introduce a rigid-body-type rotation in the "immediate" vicinity of the axis of symmetry, but that detail is omitted in Eq. (24), which is adopted at all radial positions in the gas phase. The value of the angular speed Ω is permitted to vary with time into the burn. However, Ω is taken not to vary significantly during particle flight in the present quasisteady approach, in which the particles are tracked in a temporally invariant gas-phase flowfield.

The particle trajectories under Stokes drag are described by the following dynamical balances in the axial, radial, and azimuthal directions, respectively:

$$\mu\ddot{Z}_{nm}=D\left[u(Y_{nm},Z_{nm})-\dot{Z}_{nm}\right]-\mu g \qquad (25)$$

$$\mu(\ddot{Y}_{nm}-Y_{nm}\dot{\theta}_{nm}^2)=D\left[v(Y_{nm},Z_{nm})-\dot{Y}_{nm}\right] \qquad (26)$$

$$\mu(Y_{nm}\ddot{\theta}_{nm}+2\dot{Y}_{nm}\dot{\theta}_{nm})=D\left[w(Y_{nm},Z_{nm})-Y_{nm}\dot{\theta}\right] \qquad (27)$$

where the second term on the left-hand side of Eq. (26) is the centripetal acceleration, and the second term on the left-hand side of Eq. (27) is the Coriolis acceleration. A gravitational acceleration $-g\hat{x}$ for a nosedown/nozzle-up burn has been included in Eq. (25). (In general, the residence time of particles in the motor cavity is too brief for gravitational acceleration to be of appreciable significance, although the paths of very large particles formed far upwind in the cavity might be perturbed.) The associated initial conditions are

$$Z_{nm}(t_m)=X_n(t_m)=X_{nm}, \qquad \dot{Z}_{nm}(t_m)=0 \qquad (28)$$

$$Y_{nm}(t_m)=R_{nm}, \qquad \dot{Y}_{nm}(t_m)=0, \qquad \dot{\theta}(t_m)=\Omega(t_m)=\Omega_m \qquad (29)$$

The set of Eqs. (25-27) is of fifth order, in that the particular value of θ itself is without consequence in an azimuthally symmetric process. Since a mechanism (centripetal acceleration) for the radial motion of a particle away from the axis of symmetry now complements a mechanism (interphase drag) for the radial motion of a particle toward the axis, even for a

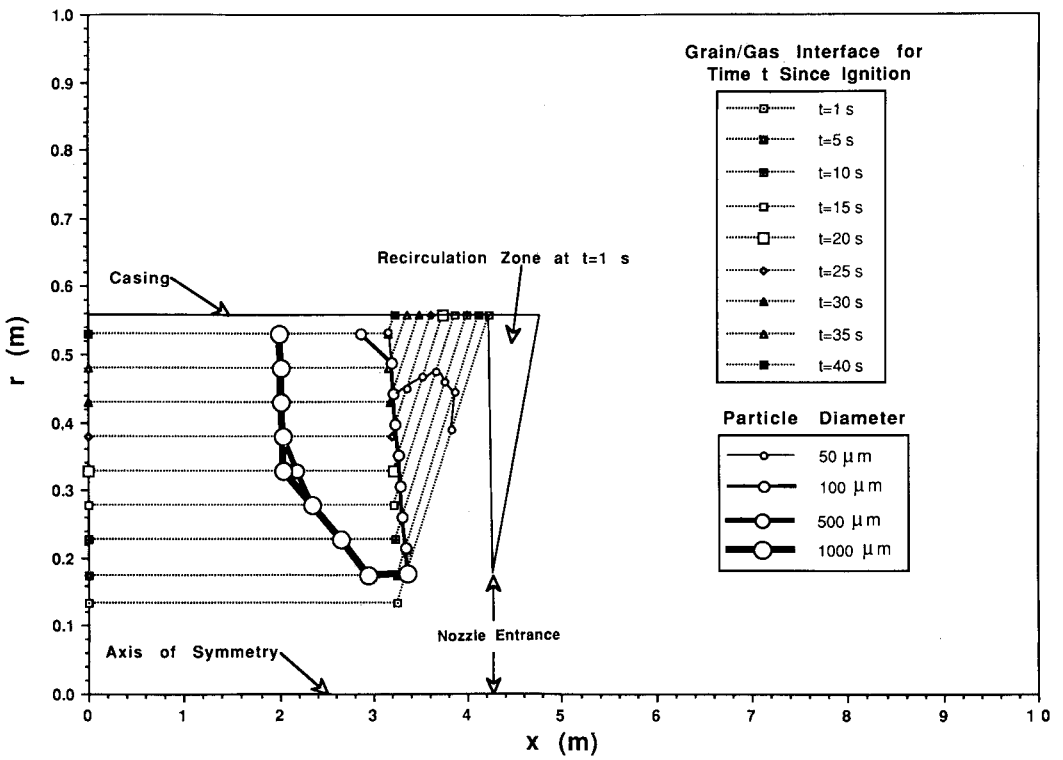

Fig. 11 The temporal evolution of the gas/grain interface, and of the "separatrices" that distinguish the motor-exiting particles emerging more upwind along the interface from nonexiting particles emerging more downwind, for four particle sizes, for the case of Eq. (31). For this shorter geometry, more particles fail to exit the motor.

monodisperse distribution of particle sizes, the possibility of intersecting trajectories (and particle collisions) should be noted, and special provisions may be required in particular circumstances. However, in general, the intersection of particle trajectories does not necessarily imply significant particle-particle collisions, since the particles are discrete.

VIII. Numerical Examples

For a given set of input parameters (such that the geometry of the casing and nozzle, together with the burn rate of the grain $\dot{R}_s$ and the spatial extent of the recirculatory-flow zone F are given), the trajectories of particles emerging from typically 19 fairly uniformly distributed sites along the gas/grain interface are tracked at each of typically nine prespecified uniformly distributed times (after ignition and during the burn). Furthermore, at each of the approximately nine times, typically four sizes of particles are tracked, such that the range from nearly velocity-slip-free to highly slip-prone behavior is encompassed. (The slip-free-particle trajectories delineate the streamlines of the flow.) The computing of the 19 trajectories (for a given particle size at a given time into the burn of a given rocket motor) requires about 1 min on a Perkin Elmer 3230 minicomputer, which is roughly comparable to a VAX 780. The results to be reported here are based on the gas-phase-flowfield description given in the Appendix, with the (modestly) enhanced regression rate for the conically configured portion of the gas/grain interface $\dot{R}_s^*$ so chosen that the results are effectively equivalent to those obtained by the procedures of Sec. IV for a plausible star-shaped configuration for the downwind portion of the grain.

The following *baseline* parameter assignments (for a purely hypothetical solid rocket motor) hold for all reported results unless explicit statement is made to the contrary (ignition is recalled to occur at time $t = 0$):

$$p_0 = 10.07 \text{ MPa}, \quad T_0 = 3650 \text{ K}, \quad \rho_g = 9.287 \text{ kg/m}^3$$

$$\rho_1 = 1295 \text{ kg/m}^3, \quad \rho_s = 3965 \text{ kg/m}^3, \quad F = 1$$

$$\dot{R}_s = 1.016 \times 10^{-2} \text{ m/s}, \quad \dot{R}_s^* = 1.03 \times 10^{-2} \text{ m/s}$$

$$L = 6.299 \text{ m}, \quad R_0 = 0.127 \text{ m}, \quad R_2 = 0.5588 \text{ m}$$

$$R_3 = 0.2032 \text{ m}, \quad x_1(0) = 3.645 \text{ m}, \quad x_2(0) = 6.02 \text{ m}$$

$$x_3 = 6.02 \text{ m} \tag{30}$$

The value adopted for ρ_s is for ambient conditions; a smaller value may hold in motors. The time to burn through the bore t_f is computed to be 42.5 s. The implicit consistent value for the density of the metallized-composite grain is about $1.5\rho_1 \doteq 1850$ kg/m^3.

A *modified* set of parameters retains the assignment of Eq. (30) except that

$$L = 4.775 \text{ m}, \quad R_0 = 0.1245 \text{ m}, \quad R_2 = 0.5588 \text{ m}$$

$$R_3 = 0.1778 \text{ m}, \quad x_1(0) = 3.264 \text{ m}, \quad x_2(0) = 4.254 \text{ m}$$

$$x_3 = 4.267 \text{ m} \tag{31}$$

For a purely *cylindrical* grain, one again adopts Eq. (30), except that now [$x_2(0)$, $\dot{R}_s^*$, F become irrelevant]

$$x_1(0) = x_3 = 3.645 \text{ m} \tag{32}$$

In the sense that it is inefficient not to fill the entire cavity with grain, the geometries being examined through this paper actually pertain to times slightly after ignition, i.e., after the recessed cavity has been burned out. The preponderance of the nonexiting slag is believed to be accumulated over the interval of the burn that is encompassed by the model.

Results are sought here for time $t = 1, 5, 10, 15, \ldots, 35, 40$ s. Particles of diameter $2a = 50$, 100, 500, and 1000 μm are examined. The only other parameter variation reported is comparing results for $F = 1$ and $F = 0.75$.

Figures 7–9 present particle trajectories for the baseline parameter assignments [Eq. (30)] for time $t = 20$ s, for particle diameters of 50, 100, and 500 μm, respectively. Figures 10–12 present the temporal evolution of the gas/grain interface, together with the temporal evolution of the "separatrices" [each of which distinguishes the upwind interface-origination sites

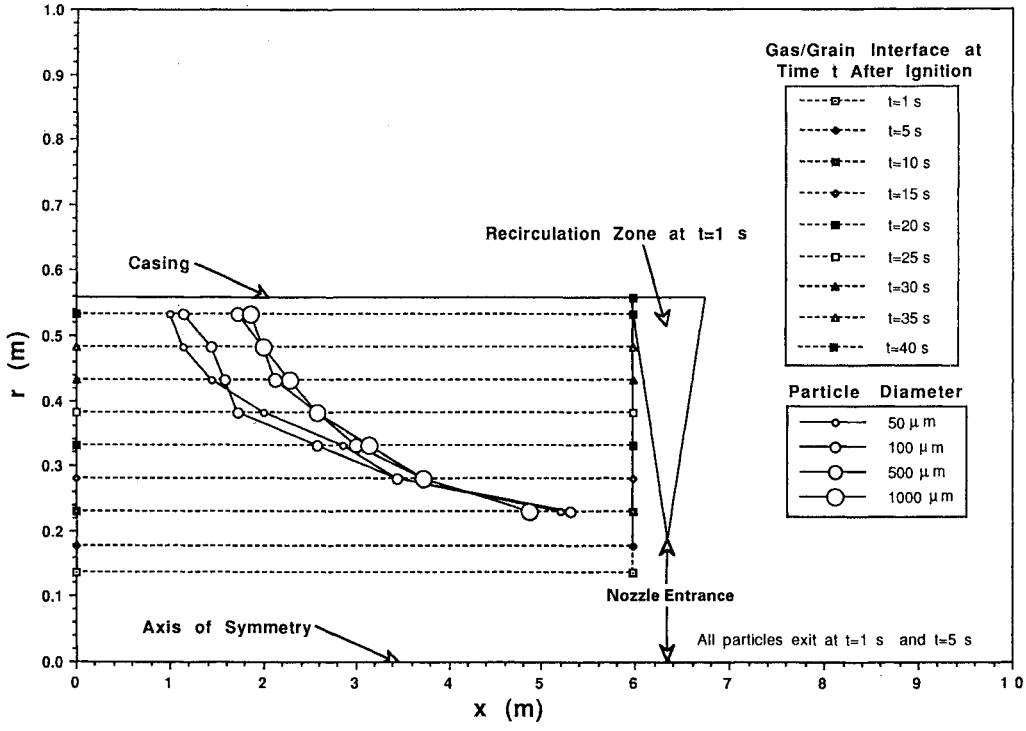

Fig. 12 The temporal evolution of the gas/grain interface, and of the "separatrices" that distinguish the motor-exiting particles emerging more upwind along the interface from nonexiting particles emerging more downwind, for four particle sizes, for the case of Eq. (32).

for particles (of a given size) that eventually exit the motor via the nozzle from the downwind interface-origination sites of identically sized particles that do not exit] for the cases of Eqs. (30), (31), and (32), respectively. Upon the adopting of a particle-size distribution, one then is able to estimate the net nonexiting grain mass. The effect of a smaller recirculatory-flow domain (as reflected in adopting a smaller value for the parameter F) is to enhance the number of larger particles that fail to exit the motor.

For the baseline parameter assignments, 500-μm or 1000-μm particles formed in the constant-bore region may be centrifuged back on to the grain-gas interface for angular velocity Ω exceeding about 2 rad/s. Generally, such rotation is limited to diagnostic firings for large motors.

IX. Future Directions

For the present approach, in which no interaction between the gas flow and the particle fields is included, the principal need is for a more adequate treatment of the gas flow in the domain $x_3 > x > x_2(t)$. Explicitly, this is the gas-filled domain extending from the downwind end of the grain to the entrance to the re-entrant nozzle. The present model seems plausible only for $F \doteq 1$, i.e., for a recirculation zone extending from the nozzle entrance upwind virtually to the end of the grain. The revised model for the nonrecirculatory portion of the gas-filled domain downwind of the end of the grain probably will retain the approximations of an incompressible, irrotational gaseous flow; what is wanted is a more physically realistic solution for this domain for conditions for which the extent of the recirculatory flow is more axially limited. (In such cases, a small particle emerging from the constant-diameter-bore grain might enter the expanded flow aft of the grain only to be "captured" by the recirculatory flow, whereas an upwind-generated large particle, never diverted, would enter the nozzle.) While retention of a radially invariant profile for the axial velocity component for the bore region $x_1(t) > x > 0$ is anticipated, inclusion of a radial variability of the axial velocity component for $x > x_1(t)$ is anticipated. Furthermore, solution may be sought not just to the nozzle entrance at $x = x_3$, but virtually to the throat of the nozzle, where smoothness constraints may be applied. In any case, once the axial component of the gas velocity is in hand, the radial component is expected to follow from conservation of mass in the small.

The following remarks outline a tentative approach to seeking a coupled-gas-solid model, appropriate for heavier particle loading. A particle-size distribution for the alumina particles that form and enter the flow at the grain-gas interface is taken as given. Also, on the basis of experience gained with the uncoupled model, one must divide the domain of the particle sizes into those with diameter $d < d_0$ and those with $d > d_0$, where $d < d_0$ encompasses particles whose paths differ from the gas streamline (emerging coincidentally from the gas-grain interface) by an ignorable discrepancy. The "gas" is to be regarded as that material which comprises the actual gas plus the $d < d_0$ particles. Of course, in doing so, one defines density as the mass of this composite medium per volume of space. One calculates the initial approximation to the gas flow exactly as one would in the particle-free case, and this statement applies whether or not an improved aft-end treatment is part of the procedure.

One then undertakes Lagrangian particle-trajectory tracking to obtain a lowest-order estimation of those trajectories arising for a discretized set of particles sizes lying in the range $d > d_0$. The only subtle consideration concerns the drag coefficient. If large particles are traversing the gas, those large particles encounter, and perhaps sweep up, some small particles. The rate of momentum transfer to the large particle is then the product of the rate at which the large particle encounters the small-particle mass times the change in the small-particle speed; i.e., under a basic Stokes drag ($d = 2a$)

$$\mu \dot{v} = 6\pi\mu_g\left(\frac{d}{2}\right)(u - v) + \rho_{sp}\left(\frac{\pi d^2}{4}\right)(u - v)|u - v| \tag{33}$$

Explicitly, here u is the gas velocity, v is the particle velocity, and ρ_{sp} is the mass per unit volume of space of the small-particle part of the gas. Probably the effective (capture) frontal area of the large particle is less than the factor $(\pi d^2/4)$, which appears in Eq. (33), but further refinement is deferred.

Given the trajectories of the large particles, one must back out the force per unit volume exerted on the gas by those particles. For this purpose one needs the number density N_n for each member n of the discrete spectrum of (large) particle sizes. The force per unit volume on the gas is then given by the expression

$$-\sum_n N_n \rho_{sp}\left(\frac{\pi d_n^2}{4}\right)(u - v)|u - v| \tag{34}$$

Upon averaging over each in-motor cross section, one can compute the upwind-directed force per unit volume on the gas, a quantity that may be equated to the axial pressure gradient. This calculation indicates whether the streamwise variation of pressure at a given time needs to be accounted for, in an upgraded treatment of the phenomenon.

Appendix: Closed-Form Expressions for the Gas-Phase Velocity Field

The formulas of Sec. IV yield numerically tabulated results for the gas-phase radial and axial velocity components (v and u, respectively) for use in the Lagrangian-particle-trajectory calculations [say, Eqs. (18) and (19)]. As noted in the third paragraph of Sec. III, alternative, convenient, closed-form expressions are readily available if one takes the mass transfer from the star-configured portion of the grain to be satisfactorily approximated by a conical, axisymmetric geometry with a solid-fuel-surface regression rate $\dot{R}_s^*$ (with units of velocity) *enhanced* relative to the burn rate $\dot{R}_s$ in the bore zone. Both $\dot{R}_s$ and $\dot{R}_s^* (> \dot{R}_s)$ are (given) constants. It follows geometrically (Fig. 5) that, if R_0 is the bore radius at time $t = 0$,

$$\tan\Phi = \frac{R_2 - R_0}{x_2(0) - x_1(0)} \tag{A1}$$

$$x_2(t) = x_1(0) + \frac{R_2 - R_0}{\tan\Phi} - \frac{\dot{R}_s^* t}{\sin\Phi} \tag{A2}$$

$$x_1(t) = x_1(0) + \frac{1}{\tan\Phi}\left(\dot{R}_s t - \frac{\dot{R}_s^* t}{\cos\Phi}\right) \tag{A3}$$

There is no grain left in the bore at time $t_f = (R_2 - R_0)/\dot{R}_s$; also, $x_2(t) \to x_1(t)$ as $t \to t_f$; in practice, $t_f > t_{bd}$ where $x_1(t_{bd}) = 0$.

In the star region II [i.e., in $x_2(t) > x > x_1(t)$, $R(x,t) > r > 0$],

$$R(x,t) = R_0 + [x - x_1(0)]\tan\Phi + \frac{\dot{R}_s^*}{\cos\Phi} t \tag{A4}$$

$$A(x,t) = \pi R^2(x,t), \qquad P(x,t) = 2\pi R(x,t) \tag{A5}$$

Equations (A4) and (A5) holds in the bore region I [i.e., in $x_1(t) > x > 0$, $R(t) > r > 0$] except that $\dot{R}_s^* \to \dot{R}_s$ and $\Phi = 0$. Equations (7c), (6c), and (5) yield $u(x,t)$ and $v(r,x,t)$ for both regions.

In region III, i.e., in $\{x_3 - [x_3 - x_2(t)]F\} > x > x_2(t)$, $R_2 > r > 0$, $A = \pi R_2^2$, $P = 2\pi R_2$, $\dot{R}_s = 0$, $v(r,x,t) = 0$, and

$$u(x,t) = u_2[x_2(t), t] \tag{A6}$$

The constant factor F is discussed in Sec. IV.

In region IV, i.e., in $\{x_3-[x_3-x_2(t)]F\}<x<x_3$, $R>r>0$, $\dot{R}_s=0$, Eq. (A5) holds, and

$$R(x,t)=\frac{R_3-R_2}{[x_3-x_2(t)]F}x+\frac{x_3R_2-\{x_3-[x_3-x_2(t)]F\}R_3}{[x_3-x_2(t)]F} \tag{A7}$$

Again, Eqs. (7c), (6b), and (5) yield u and v.

In the recirculation zones V and VI, $u=v=0$. Since a particle entering these zones will not leave the motor, the only motivation for continuing a particle-trajectory calculation is to identify the site of impact with the inner lining of the casing.

The patching of piecewise approximations to the velocity components does imply discontinuous slope at interfaces, but such local anomalies seem of minor consequence for particle-trajectory tracking.

Acknowledgments

The authors are grateful to James Kliegel of the TRW Defense Systems Group in San Bernardino, California, for suggesting the problem, for helpful input, and for allocating the necessary resources. They also thank Ethel Johnson for her help.

References

[1]Price, E. W., "Combustion of Metallized Propellants," *Progress in Astronautics and Astronautics: Fundamentals of Solid-Propellant Combustion,* Vol. 90, AIAA, New York, 1984, pp. 479-513.

[2]Kliegel, J. R., "Gas-Particle Nozzle Flow," *Ninth Symposium (International) on Combustion,* Academic, New York, pp. 811-826.

[3]Waesche, R. H. W., Sargent, W. H., and Marchman, J. F., "Space Shuttle Rocket Motor Aft-End Internal Flows," *Journal of Propulsion and Power,* Vol. 5, Nov.-Dec. 1989, pp. 650-656.

[4]Crowe, C. T., "REVIEW—Numerical Models for Dilute Gas-Particle Flow," *Journal of Fluid Engineering,* Vol. 104, Sept. 1982, pp. 297-303.

[5]Batchelor, G. K., *An Introduction to Fluid Dynamics,* 1st ed., Cambridge Univ., Cambridge, England, UK, 1977, pp. 536-538.

[6]Haloulakos, V. E., and Davis, J. C., "Slag Formation Analysis," McDonnell Douglas Astronautics Co., Huntington Beach, CA, MDC G8864, Jan. 1983.

[7]Haloulakos, V. E., "Rocket Motor Slag Formation: Effects of Internal Flow Field and Propellant Grain Configuration," McDonnell Douglas Astronautics Co., Huntington Beach, CA, MDC H1422, Feb. 1985.

[8]Haloulakos, V. E., "Slag Mass and Two-Phase Nozzle FlowAsymmetry Effects on Rocket Motor Performance," McDonnell Douglas Astronautics Co., Huntington Beach, CA, MDC H1543, July 1986.

[9]Golafshani, M., and Loh, H. T., "Computation of Two-Phase Viscous Flow in Solid Rocket Motors Using a Flux-Split Eulerian-Lagrangian Technique," AIAA Paper 89-2785, July 1989.

[10]Chang, I-S., "One- and Two-Phase Nozzle Flows," *AIAA Journal,* Vol. 18, Dec. 1980, pp. 1455-1461.

[11]Hwang, C. J., and Chang, G. C., "Numerical Study of Gas-Particle Flow in a Solid Rocket Nozzle," *AIAA Journal,* Vol. 26, June 1988, pp. 682-689.

[12]Culick, F. E. C., "Rotational Axisymmetric Mean Flow and Damping of Acoustic Waves in a Solid Propellant Rocket," *AIAA Journal,* Vol. 4, Aug. 1966, pp. 1462-1464.

[13]Goldstein, S., *Lectures on Fluid Mechanics,* 1st ed., Interscience, London, 1960, pp. 115-116.

[14]Rudinger, G., *Fundamentals of Gas-Particle Flow,* 1st ed., Elsevier, New York, 1980, pp. 7-39.

[15]Bird, R. B., Stewart, W. E., and Lightfoot, E. N., *Transport Phenomena,* 1st ed., Wiley, New York, 1960, pp. 190-194.

[16]Fernandez de la Mora, J., and Riesco-Chueca, P., "Aerodynamic Focusing of Particles in a Carrier Gas," *Journal of Fluid Mechanics,* Vol. 195, Oct. 1988, pp. 1-24.